Carbohydrate Polymers 226 (2019) 115261

Contents lists available at ScienceDirect

Carbohydrate Polymers

journal homepage: www.elsevier.com/locate/carbpol

Polyphosphonium-oligochitosans decorated with nanosilver as new prospective inhibitors for common human enteric viruses

Ahmed R. Sofy[a,*], Ahmed A. Hmed[a], Naglaa F. Abd El Haliem[b], Mohamed A.-E. Zein[c], Reda F.M. Elshaarawy[d,e,**]

[a] Botany and Microbiology Department, Faculty of Science, Al-Azhar University, 11884 Nasr City, Cairo, Egypt
[b] Microbiology and Immunology Department, Faculty of Medicine (Girls), Al-Azhar University, Nasr City, Cairo, Egypt
[c] Faculty of Science, Chemistry Department, Damanhour University, Egypt
[d] Institut für Anorganische Chemie und Strukturchemie, Heinrich-Heine Universität Düsseldorf, 40204 Düsseldorf, Germany
[e] Faculty of Science, Suez University, Suez, Egypt

ARTICLE INFO

Keywords:
Polyphosphonium oligochitosans
Nanosilver-based biocomposites
Antiviral
Enterovirus replication inhibitors

ABSTRACT

The main objective of this work to explore new safe antiviral agents against hepatitis A virus (HAV), norovirus (NoV) and Coxsackievirus B4 (CoxB4) infections. In this context, we have successfully prepared new poly-quaternary phosphonium oligochitosans ($PQPOC_{1,2}$) to use them as natural synergistic *in-situ* bioreductants of silver ions into nanosilver and stabilizing agent for these nanosilver to fabricate PQPOCs-AgNPs nano-biocomposites (NBC1,2). The antiviral performance of the PQPOCs and NBCs against FCV, HAV, and CoxB4 reflects great virucidal activities for NBCs as compared with PQPOCs with maximum viral reduction% (41.42, 80.62, and 84.04%) for NBC1 against FCV, HAV, and CoxB4, respectively. Furthermore, the antiviral activity of NBC1 is concentration- / pH-dependent where NBC1 acquired its maximum antiviral at [NBC1] = 200 μL/mL and pH 4. Based upon these facts, we could attribute the enhanced virucidal efficacy of NBC1: (i) binding of AgNPs to the virions active sites. (ii) Electrostatic interaction between the positive brushes of PQPOC and negative targets of viruses. (iii) Inducing ribonuclease catalyzed by CS to degrade the viral RNA and consequently prevents its transcription and translation.

1. Introduction

Enteric viruses play a pivotal role in food-/water-borne diseases (FBDs/ WBDs) outbreaks (Lodder, van den Berg, Rutjes, & de Roda Husman, 2010; Prevost et al., 2015). Among these FB/WB viruses, hepatitis A virus (HAV) and enterovirus (EV) such as human norovirus (NoV) and Coxsackievirus B4 (CoxB4) have attracted the interest of numerous researchers due to their serious impacts on public health and environment (Sofy et al., 2018a, 2018b; Haas, Rose, Gerba, & Regli, 1993; EFSA, 2016). Globally, it was found that 120 million FBDs were caused by viral contamination of food, annually (WHO, 2015). Most of these viruses have no licensed antiviral drug. Thus, there is an imperative need for exploring new effective and safe therapeutics for these FB viruses, particularly for NoV. In this context, a great interest was directed toward natural compounds as antiviral candidates. Natural biopolymers potentially have synergistic multifunctions, not only to enhance the quality and safety of food products but also to serve as natural antivirals (Randazzo, Fabra, Falcó, López-Rubio, & Sánchez, 2018).

Amongst natural biopolymers, the inherent biodegradability, biocompatibility, antimicrobial, antiviral and antibiofilm efficacies, non-toxicity and eco-friendship of chitosan (CS) biopolymer (Randazzo et al., 2018; Elshaarawy, Refaee, & El-Sawi, 2016; Guan et al., 2019) make it a promising scaffold for constructing of new smart pharmacological materials. Nevertheless, the widespread application of native CS as a pharmacological agent is restricted due to its poor aqueous solubility and thus limited bioavailability, low thermal and mechanical stability. Surface-functionalization of CS acts as the magic solution to tackle these challenges (Elshaarawy, Mustafa, Herbst, Farag, & Janiak, 2016, 2018). Notably, our earlier outputs (Elshaarawy, Mustafa et al., 2016; Elshaarawy & Janiak, 2014; Elshaarawy et al., 2017) revealed that decoration of the pharmacological molecules with ionic liquid (IL)

* Corresponding author.
** Corresponding author at: ARS, Botany and Microbiology Department, Faculty of Science, Al-Azhar University, 11884 Napa City, Cairo, Egypt; RFME, Institut für Anorganische Chemie und Strukturchemie, Heinrich-Heine Universität Düsseldorf, 40204 Düsseldorf, Germany.
E-mail addresses: ahmed_sofy@azhar.edu.eg (A.R. Sofy), reel-001@hhu.de, reda.elshaarawy@suezuniv.edu.eg (R.F.M. Elshaarawy).

https://doi.org/10.1016/j.carbpol.2019.115261
Received 10 June 2019; Received in revised form 20 July 2019; Accepted 27 August 2019
Available online 28 August 2019

motifs resulting in synergetic effects of amelioration the aqueous solubility and significant enhancement of the antimicrobial performance.

Through the last few decades, silver nanoparticles (AgNPs) have become in the forefront of metal NPs-based biomedical materials because of their unmatched properties including ease of the fabrication with low cost, great surface area and remarkable broad-spectrum antimicrobial activities (Durán, Nakazato, & Seabra, 2016). Thus, AgNPs-based materials always offered interesting, challenging, and promising characteristics suitable for diverse applications. Notablly, AgNPs-based antiviral agents are incredibly useful in combating many viruses such as Adenovirus (Chen, Zheng, Yin, Li, & Zheng, 2013), Bovine herpesvirus-1 (El-Mohamady, Ghattas, Zawrah, & Abd El-Hafeiz, 2018), Coxsackievirus B3 (Shaheen, El-hadedy, & Ali, 2019), Chikungunya (Sharma et al., 2019), Hepatitis B (Lu et al., 2008), Human parainfluenza type 3 (Gaikwad et al., 2013), Human immunodeficiency virus type 1 (Trefry & Wooley, 2013), Influenza A (Park et al., 2018; Park et al., 2018), and Monkeypox (Rogers, Parkinson, Choi, Speshock, & Hussain, 2008). Also, AgNPs may block viral receptors and/or interfere with the viral genome when a virus enters the host cells, by inactivating viral particles outside the host cells (Khandelwal, Kaur, Kumar, & Tiwari, 2014). Unfortunately, the widespread biomedical applications of AgNPs are restricted by their hygienic and environmental problems (Leon-Silva, Fernandez-Luqueno, & Lopez-Valdez, 2016). Whereas the leaching of Ag(I) ions from the surface of AgNPs (Gaillet & Rouanet, 2015) and their agglomeration into bulky particles or fibers, may fluctuate their biological features and cause serious impacts upon the environment and the human health (Ray, Yu, & Fu, 2009). Therefore, exploring novel, innovative strategies for enveloping and stabilization of AgNPs is an urgent need to overcome these obstacles.

Despite extensive work has been reported to prepare AgNPs using CS as synergistic reducing, enveloping and stabilizing agents (Bui, Park, & Lee, 2017; Kalaivani et al., 2018; Murugadoss & Chattopadhyay, 2008), however, no attention has been paid toward the utilization of poly quaternary phosphonium (PQP)-based CS as a synergistic reductant and capping agent. Noteworthy that the triphenylphosphonium (TPP)-based quaternary phosphonium salts (QPS) possess unique structural features which enable them to form delocalized lipophilic cations (Wang, Shao, Zhang, & Cheng, 2014; Wang, Xu, Zhao, & Zhao, 2014). Also, TPP can preferentially migrate from an aqueous to the hydrophobic environment and selectively accumulate in the mitochondria of pathogenic cells because of their higher trans-membrane potentials in comparison to the normal cells (Biswas, Dodwadkar, Piroyan, & Torchilin, 2012; Boddapati et al., 2005; Yamada & Harashima, 2008). As a result, TPP can offer promising motifs for fine-tuning of the structural features of different polymers to achieve drug targeted delivery (Wang, Shao et al., 2014, 2014b; Zhang et al., 2015; Wang et al., 2013; Zhou et al., 2013).

Inspired by the aforementioned amazing facts, the present study is aimed mainly to *in-situ* prepare and stabilize AgNPs using new PQP-based oligochitosans (PQPOCs), safe smart materials, which act as synergistic reductant and encapsulating agents and thus tightly adhere AgNPs to fabricate novel nanobiocomposites (NBCs) for antiviral applications.

2. Materials and methods

2.1. Experimental protocol

Extraction of CS from marine wastes and its partial de-polymerization into oligochitosan (OC) were carried out according to our earlier work (Elshaarawy et al., 2017). Materials and experimental methods for preparation of TPP salts (**2a,b**) along with the different techniques for comprehensive characterization of all synthesized material were described in the electronic supplementary material (ESM).

2.1.1. Preparation of PQPOCs

Generally, a 25 ml ethanolic solution of TPP salts (**2a,b**) (equivalent to molar NH_2-content in OC which can be calculated from N% in OC) was added dropwise to a 75 mL of a 50% (v/v) mixed-solvent (2% $AcOH_{aq}$/ EtOH) solution containing 1 g of OC under vigorous stirring at 70 °C. Then the solution was stirred for more 24 h at the same conditions. Thereafter, the reaction mixture was concentrated under reduced pressure to give a gel-like residue which diluted with an excessive amount of ethyl acetate (AcOEt) and ultrasonically irradiated for 1 h to remove the solvent and solidify these gel-like products. The isolated solids were filtered and washed with EtOH:AcOEt mixtures (30:70, 20:80, and 0:100 V/V, sequentially). Finally, the desired products $PQPOC_{1,2}$ were dried at 35 °C under vacuum for 24 h and characterized as follows;

***Poly-N-(((3-(3-hydroxy-4-(1-iminoethyl)phenoxy)propyl)triphenylphosphonium chloride) oligochitosan (PQPOC$_1$)*:** Canary yellow powder, Yield (1.72 g). ATR-FTIR (cm^{-1}): 3384 (m, br, $\nu_{(O\text{-}H\ +\ NH2)}$), 3229 (m, sh, $\nu_{(N\text{-}H)}$), 3096 (m, br, $\nu_{(Ar\text{-}H)}$), 2956 (m, br, $\nu_{(C\text{-}H)}$), 1638 (vs, sh, $\nu_{(C=O\ +\ C=N)}$), 1588 (vs, sh, $\nu_{(amide\ II)}$), 1537 (m, sh), 1454 (s, sh, $\nu_{(Ar\text{-}P)}$), 1382 (s, sh, $\nu_{(amide\ III)}$), 1275 (m, sh, $\nu_{(Ar^{-}O)}$), 1112 (s, sh, $\nu_{(Ar\text{-}P+Cl-)}$), 1082 (s, sh), 893 (s, sh $\nu_{(C\text{-}O\text{-}C)}$, β-glycosidic linkage), 736 (s, sh). ^{1}H NMR (600 MHz, 1% $CD_3COOD/D_2O)_{60°C}$ δ (ppm): 10.27 (s, 2H, 2 x O-H), 8.21 (s, 1H, N-H), 7.72 (d, J = 7.0 Hz, 2H, 2 x Ar-H), 7.65 (d, J = 7.1 Hz, 12H, 12 x Ar-H), 7.58-7.39 (m, 12H, 12 x Ar-H), 7.35-7.18 (m, 12H, 12 x Ar-H), 6.87 (d, J = 6.8 Hz, 2H, 2 x Ar-H), 6.58 (s, 2H, 2 x Ar-H), 5.63 (s, br, 4H, chitosan-H), 4.26 (t, J = 1.5 Hz, 4H, 2 x Ar-O-CH_2), 4.18-3.91 (m, 12H, chitosan-H), 3.83 (s, br, 4H, chitosan-H), 3.75 (t, J = 7.0 Hz, 4H, chitosan-H), 3.66 (s, br, 4H, chitosan-H), 3.56-3.35 (m, 8H, chitosan-H), 3.05 (t, J = 6.9 Hz, 4H, chitosan-H), 2.51 (t, J = 1.4 Hz, 4H, 2 x $^+$P-C**H**$_2$CH$_2$), 2.22-2.08 (m, 4H, 2 x Ar-O-CH$_2$C**H**$_2$CH$_2$), 1.96-1.86 (m, 4H, 2 x $^+$P-CH$_2$C**H**$_2$CH$_2$), 1.84 (s, 3H, NHAc), 1.82 (s, 6H, 2 x CH_3), 1.32-1.18 (m, 4H, 2 x Ar-O-CH$_2$C**H**$_2$CH$_2$). ^{13}C NMR (151 MHz, 1% $CD_3COOD/D_2O)_{60°C}$ δ (ppm): 175.68 (C = O), 164.79 (C = N), 163.81 (phenoxy C-O), 162.05 (phenolic C-OH), 136.43 (Ar-C), 132.13 (Ar-C), 131.09 (Ar-C), 129.96 (Ar-C), 118.77 (Ar-C), 117.32 (Ar-C), 112.10 (Ar-C), 109.71 (Ar-C), 109.65 (Ar-C), 108.41 (chitosan-C), 105.14 (chitosan-C), 87.78 (chitosan-C), 82.89 (chitosan-C), 82.78 (chitosan-C), 81.83 (chitosan-C), 81.71 (chitosan-C), 80.23 (chitosan-C), 79.69 (chitosan-C), 78.93 (chitosan-C), 75.91 (chitosan-C), 75.08 (chitosan-C), 71.95 (chitosan-C), 71.45 (chitosan-C), 68.93 (Ar-O-**C**H$_2$), 65.13 (chitosan-C), 63.05 (chitosan-C), 62.91 (chitosan-C), 62.88 (chitosan-C), 61.82 (chitosan-C), 59.11 (chitosan-C), 56.65 (chitosan-C), 54.62 (chitosan-C), 30.48 (Ar-O-CH$_2$**C**H$_2$), 29.99 (Ar-O-CH$_2$CH$_2$**C**H$_2$), 23.86 (CO**C**H$_3$), 22.78 ($^+$P-CH$_2$**C**H$_2$), 22.39 ($^+$P-**C**H$_2$CH$_2$) and 18.51 (CH_3). ^{31}P NMR (202 MHz, CD_3COOD/D_2O): 32.52 ppm (singlet, Ph_3P^+).

***Poly-N-((3-(3-hydroxy-4-(1-iminoethyl) phenoxy)propyl)triphenylphosphonium hexafluoro- phosphate) oligochitosan (PQPOC$_2$)*:** Yellow powder, Yield (1.76 g). ATR-FTIR (cm^{-1}): 3420 (m, br, $\nu_{(O\text{-}H\ +\ NH2)}$), 3247 (m, sh, $\nu_{(N\text{-}H)}$), 3056 (m, br, $\nu_{(Ar\text{-}H)}$), 2962 (m, br, $\nu_{(C\text{-}H)}$), 1639 (vs, sh, $\nu_{(C=O\ +\ C=N)}$), 1592 (vs, sh, $\nu_{(amide\ II)}$), 1537 (m, sh), 1439 (s, sh, $\nu_{(Ar\text{-}P)}$), 1385 (s, sh, $\nu_{(amide\ III)}$), 1279 (m, sh, $\nu_{(Ar^{-}O)}$), 1149 (s, sh), 1074 (s, sh), 891 (s, sh $\nu_{(C\text{-}O\text{-}C)}$, β-glycosidic linkage), 832 (vs, sh, $\nu_{(PF6+)}$), 738 (s, sh). ^{1}H NMR (600 MHz, 1% $CD_3COOD/D_2O)_{60\ °C}$ δ (ppm): 10.28 (s, 2H, 2 x O-H), 8.11 (s, 1H, N-H), 7.68 (d, J = 7.0 Hz, 2H, 2 x Ar-H), 7.68 (d, J = 7.1 Hz, 12H, 12 x Ar-H), 7.61-7.40 (m, 12H, 12 x Ar-H), 7.37-7.19 (m, 12H, 12 x Ar-H), 6.86 (d, J = 6.9 Hz, 2H, 2 x Ar-H), 6.59 (s, 2H, 2 x Ar-H), 5.61 (s, br, 4H, chitosan-H), 4.28 (t, J = 1.4 Hz, 4H, 2 x O-CH$_2$), 4.20-3.98 (m, 12H, chitosan-H), 3.82 (s, br, 4H, chitosan-H), 3.77 (t, J = 6.9 Hz, 4H, chitosan-H), 3.65 (s, br, 4H, chitosan-H), 3.56-3.36 (m, 8H, chitosan-H), 3.09 (t, J = 6.8 Hz, 4H, chitosan-H), 2.53 (t, J = 1.3 Hz, 4H, 2 x $^+$P-C**H**$_2$CH$_2$), 2.21- 2.06 (m, 4H, 2 x O-CH$_2$C**H**$_2$CH$_2$), 1.94-1.85 (m, 4H, 2 x $^+$P-CH$_2$C**H**$_2$CH$_2$), 1.83 (s, 3H, NHAc), 1.81 (s, 6H, 2 x CH_3), 1.33-1.17 (m, 4H, 2 x O-CH$_2$C**H**$_2$CH$_2$). ^{13}C NMR (151 MHz, 1% $CD_3COOD/D_2O)_{60°C}$ δ (ppm): 174.99, 165.12, 163.73, 161.85, 136.43, 132.21, 131.04, 130.01,

118.68, 117.31, 112.24, 109.58, 109.52, 108.39, 105.23, 87.75, 82.81, 82.77, 81.85, 81.63, 80.23, 79.59, 78.93, 75.87, 75.08, 71.83, 71.45, 68.93, 65.13, 63.05, 62.91, 62.88, 61.82, 59.17, 57.00, 55.12, 30.33, 30.02, 23.85, 22.75, 22.61 and 18.48. ^{31}P NMR (202 MHz, DMSO-d_6): 32.52 ppm (singlet); –142.96 ppm (septet, $^2J_{PF}$ = 711.23 Hz). ^{19}F NMR (470 MHz, CD_3COOD/D_2O): –70.59 ppm (doublet, $^1J_{FP}$ = 715.68 Hz).

2.1.2. In-situ green synthesis of PQPOCs-capped AgNPs

0.2 g of PQPOCs was dissolved in 100 mL of Milli-Q water containing 200 µL of NaOH solution (0.3 M) under stirring at 93–95 °C for 2 h (to ensure maximum deprotonation of the phenol group). After complete dissolution, the solution was cooled to room temperature and then a freshly prepared $AgNO_3$ solution (0.1 M. 3 mL) was added dropwise to a PQPOCs solution kept under continuous stirring for a further 30 min at the same temperature. The color of the solution was changed from light yellow to orange-yellow. Thereafter, the temperature of the reaction mixture was raised to 75 °C and stirred at this temperature for a further 60 min. The solution color was changed from orange-yellow to yellowish-brown verifying the growth of AgNPs. Then, the solution was centrifuged and washed five times with Milli-Q water and absolute ethanol, as well. The final products were dried under vacuum at 50 °C for 12 h and coded as $PQPOC_1$-AgNPs (NBC1) and $PQPOC_2$-AgNPs (NBC2).

2.2. Antiviral study

2.2.1. Viruses and cell lines

Cytopathic strain of Hepatitis A virus (HAV) was propagated in Vero cells according to Yasumura Kawakita protocol (Yasumura & Kawakita, 1963). While Coxsackie B4 virus (CoxB4) was cultivated on Hep-2 cell lines (BioWhittaker, Walkersville, MD, USA) according to Simões work (Simões, Amoros, & Girre, 1999). On the other hand and due to the deficiency of cell culture systems or animal models that can be easily used to grow Norovirus (NoV), the Feline calicivirus (FCV) can be used as an alternative for mimicking NoV activity, infection behavior, propagation and survival conditions (Jimenez & Chiang, 2006; D'Souza et al., 2006). FCV and NoV share numerous biochemical and structural features such as their similar genomic structure and sequence (3 open reading frames). So, FCV is considered as a surrogate virus for NoV in its infectivity and survival studies. FCV (ATCC® VR-2057™, strain FCV-2280) was grown in Crandell-Reese feline kidney cells (CRFK) according to earlier work (Gulati, Allwood, Hedberg, & Goyal, 2001). The cytopathic effect (CPE) of the three viruses has been detected through their culturing on their specific cell line according to the guided protocols. Microscopic examination has been carried out daily for observation of cell morphologies and cell deformation alterations. Moreover, morphological deformations such as loss of confluence, cell rounding and shrinking, and cytoplasmic granulation and vacuolization have been recorded in time intervals.

2.2.2. Cytotoxicity assay

The maximum non-toxic concentration (MNTC) (maximum concentration that has no toxic effect and unable to produce any morphological changes in the tested cells relative to the control cells, expressed in µL/mL) of the novel nano-biocomposites (NBC1,2) on Vero cells has been estimated by serial dilutions of (10–300 µL/mL). Briefly, 2×10^5 cells/mL of Vero cells were treated with the serial dilutions of the NBC in microtiter plates and have been incubated at 37 °C in a 5% CO_2 air humidified atmosphere for a further 72 h. Moreover, plates were microscopically examined in order to determine the toxic concentration of the composite through its ability to induce cell death. The 50% cytotoxic concentration of the NBC was defined based on the cell viability and their ability to cleave the tetrazolium salt, 3-(4,5-dimethylthiazol-2-yl)-2,5-diphenyl tetrazolium bromide (MTT) (Sigma, Chem, St. Louis, MO) producing formazan (Mosmann, 1983). Briefly, supernatants were removed from the wells, and 25 µL of an MTT in PBS solution (2 mg/mL) was added to each well, and the plates were incubated at 37 °C for 90 min. Then, DMSO (25 µL) was added to each well to get rid of crystallized formazan. The plates were kept for 15 min on a shaker to be ready for determination of the optical density at 492 nm (OD_{492}).

2.2.3. Antiviral assessment

The antiviral activity of PQPOCs ($PQPOC_1$ & $PQPOC_2$) and NBCs (NBC1 & NBC2) have been tested at the concentration (100 µL/mL), while, the novel most potent biocomposite (NBC1) has been tested at different serial concentrations (50, 100, 150, and 200 µL/mL) using Tissue Culture Infective Dose ($TCID_{50}$) protocol. In brief, solution of each compound (100 µL) was added to the viral suspension in PBS (200 µL, titer *ca.* $10^3 TCID_{50}$/mL) at pH 7.4. Afterward, the mixture was vigorously stirred for 10 s and left for 60 min at room temperature to allow NBC↔virus mutual interaction. Thereafter, the NBC particles were removed by centrifugation for 10 min at 6000 rpm. The supernatant (50 µL) was serially diluted several times with PBS in a 96-well cell culture plate (Greiner-Bio one) containing the appropriate cells (2×10^5) to the target virus. Plates were incubated for one hour at 37 °C and 5% CO_2 to permit the viral infection. Then, a mixture of (DMEM (50 µL), trypsin (5 ppm) and BSA (0.4%)) was added to each well once infection occurred, to maintain cells, and allowed for a futher post-infection for five days. After 5-days post-infection, methanol was added to fix the surviving cells which stained using Giemsa stain solution (5%). From the number of infected wells, the $TCID_{50}$ of each solution was calculated according to Reed-Muench method (Reed & Muench, 1938). Each compound's antiviral activity is estimated from the ratio of $TCID_{50}$ of the NBC-treated supernatant to the viral control (without treatment). The infectious titers of FCV, HAV, and CoxB4 were around 10^7, 10^8, and 10^7 $TCID_{50}$ /mL, respectively.

2.2.4. pH-dependent antiviral activity study

To determine the activity of the most potent nano-biocomposite (NBC1) at different pH values, a set of test tubes divided into six groups (in each group, three tubes dedicated to each pH value) containing 9 mL sterile distilled water (DW) were prepared. All the tubes were exposed to UV (254 nm, 100 µw/mL) for 30 min before inoculation. The distribution of groups was as follows:

Group 1: *FCV;* treated with NBC1.
Group 2: *FCV;* without treatment (control).
Group 3: *HAV;* treated with NBC1.
Group 4: *HAV;* without treatment (control).
Group 5: *CoxB4;* treated with NBC1.
Group 6: *CoxB4;* without treatment (control).

A 25 µL of virus suspension (10^7, 10^8, and 10^7 $TCID_{50}$ per mL for FCV, HAV and CoxB4, respectively) was added to each set of tubes using the appropriate techniques and maintained at room temperature for 60 min. Then, 100 µL/mL of NBC1 suspension was added for each tube; while, control groups were treated with 100 µL of DW. The pH values have been adjusted by additions of citric phosphate buffer (0.1 M) to obtain pH range 3–5 while with sodium phosphate buffer (0.1 M) to get pH range 6-9. The pH values was adjusted to pH 4, 6, 7, 8 and 9 prior viricidal activity assay for each tested group. The virus dilutions were stored at room temperature for up to 60 min. Then the antiviral activity of the NBC1 at each pH value was estimated using the $TCID_{50}$ /mL. All experiments were done in triplicate.

2.3. Statistical methods

The collected data were analyzed using Statistical Package for Social Science (SPSS) for Windows version 25.0. Normality tests were used to determine whether a given set of data was normally distributed. The Shapiro Wilk test was used to check for normal distribution of data (Snedecor & Cochran, 1980). Moreover, all data were quantitatively presented. Comparing groups was done using One Way ANOVA for

comparison of quantitative data. The P value < 0.05 was considered statistically significant.

3. Results and discussion

3.1. Chemistry of synthesis protocol

Chitosan, extracted from the marine crustaceans, was used for fabrication of oligochitosan (OC), a key starting material for our work, through the $NaNO_2$-based oxidative depolymerization reaction. The amino groups and consequently the degree of acetylation of OC plays a pivotal role in its chemical modifications *via* several possible chemical strategies such as Schiff base reaction, amide reaction, *etc.*. This to synergistically improve the aqueous dispersive ability of OC and endow it more pharmacophores for enhancing of its use in bio-related applications. Schiff base condensation has been proved to be a facile and efficient strategy to modify CS surface (Antony, Arun, Theodore, & Manickam, 2019). In this context, the as-synthesized 3-(4-acetyl-3-hydroxyphenoxy)propyl)triphenylphosphonium salts (**2a,b**) were employed to impart surface functionalization of OC, covalently, *via* Schiff base condensation for production of smart green reducing and capping agents (PQPOCs) (Scheme 1) which further applied for *in-situ* biosynthesis of AgNPs. The reducing capacity of PQPOCs for Ag^+ in the synthesis of AgNPs could be attributed to the presence of labile reductive phenolic and alcoholic hydroxyl groups upon the surface of modified OC. Meanwhile, the active coordination sites such as azomethine nitrogen and phenolate oxygen scattered on the surface of PQPOCs backbone allow the concentration of Ag^+ ions to their surface through complexation reaction.

The potential mechanism for formation AgNPs mediated by PQPOCs as synergistically capping and reducing agents was depicted in Scheme 2.

3.2. Degree of acetylation (DA) and degree of substitution (iminization) (DS)

The degree of acetylation (DA) of OC and the degree of substitution (DS) in PQPOCs were calculated using its microanalytical analysis based upon our earlier work (Elshaarawy et al., 2017). The calculated values were collected in Table 1. These values are consistent with their CHN analysis.

3.3. FTIR spectral data

Notice of new stretches 1637 ± 2 and 1276 ± 1 cm^{-1} attributable for the vibration the imine (C═N) and aryl-O groups, respectively, in the FTIR spectra of PQPOCs (Fig. 1) confirms a successful covalent grafting of triphenylphosphonium salts (**2a,b**) onto the surface of OC flakes. Resumption of ν_{NH2} band to contribute in the spectra of PQPOCs, but, with a feeble intensity as compared with that of OC confirms the partial Schiff base condensation beween triphenylphosphonium salts (**2a,b**) and OC. Two prominent peaks around 1112 and 832 cm^{-1} are characteristic for Ph-P^+ and PF_6^- vibrations, respectively, of the triphenylphosphonium terminals.

Infrared spectral data collected from the FTIR spectra for $PQPOC_1$-AgNPs (NBC1) provide preliminary evidence for a successful *in-situ* green formation and capping of AgNPs. Furthermore, it gives an insight into the potential functional groups of $PQPOC_1$ backbone responsible for the reduction of Ag^+ ions and capping of AgNPs. The broadness of the imprint of the OH stretching vibration along with its positive shift in

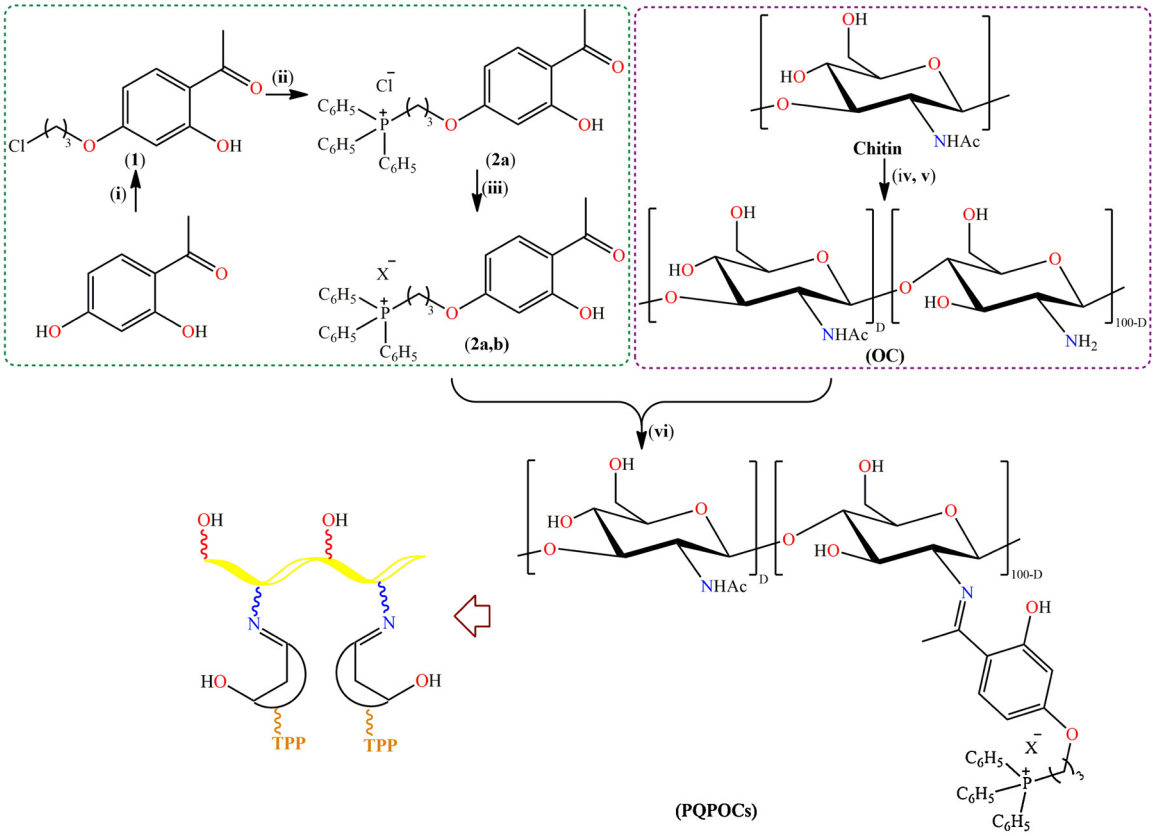

(i) 1-bromo-3-chloropropane, anhyd. K_2CO_3, dry acetone, reflux 16 h; **(ii)** Ph_3P, dry THF, reflux 3 h, N_2; **(iii)** 60% HPF_6, milli-Q water, stir, rt, 24 h; **(iv)** 65% NaOH, stir, 60 °C 72 h;**(v)** $NaNO_2$, 6% AcOH stir, rt, 3 h, pH = 7-8, $NaBH_4$, stir, rt, overnight; **(vi) 2a,b**, 50% (v/v) mixed-solvent (2% AcOHaq/ EtOH), stir, 70 °C, overnight.

Scheme 1. The schematic diagram for the preparation route of poly quaternary phosphonium-based oligochitosan (PQPOCs).

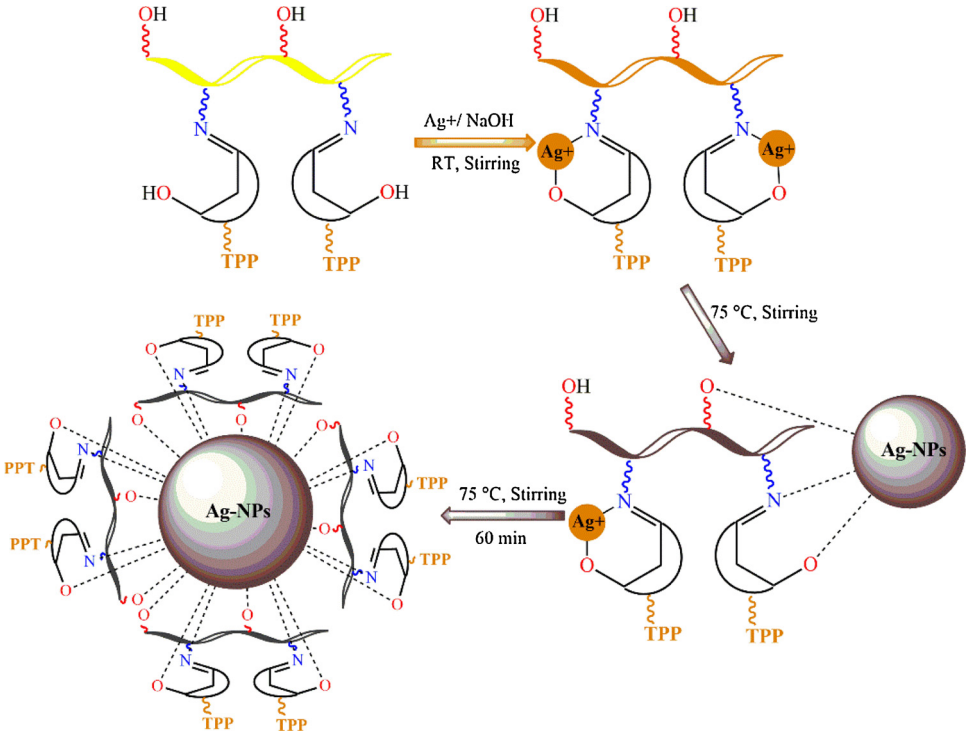

Scheme 2. Proposed mechanism for formation of AgNPs mediated by PQPOCs as synergistically capping and reducing agents.

Table 1
DA, DS and EA for proposed MF of building unit of OC and PQPOCs[a].

Sample	DA (%)	DS (%)	MF of building unit (M, g/ mol)	EA Calcd (Found) (%)		
				C	H	N
OC	26.31	–	$(C_8H_{13}NO_5)_{0.26}(C_6H_{11}NO_4)_{0.74}(H_2O)$ (190.10)	41.19 (41.24)	7.17 (7.21)	7.37 (7.29)
PQPOC$_1$	–	28.55	$(C_8H_{13}NO_5)_{0.26}(C_6H_{11}NO_4)_{0.45}(C_{35}H_{37}ClNO_6P)_{0.29}(H_2O)$ (324.03)	54.90 (54.85)	6.48 (6.51)	4.24 (4.32)
PQPOC$_2$	–	27.08	$(C_8H_{13}NO_5)_{0.26}(C_6H_{11}NO_4)_{0.47}(C_{35}H_{37}F_6NO_6P_2)_{0.27}(H_2O)$ (355.79)	50.00 (49.86)	5.90 (5.95)	3.86 (3.84)

[a] DA = Degree of acetylation; DS = Degree of substitution; EA = Elemental analysis; MF = Molecular formula; OC = Oligochitosan; PQPOC = poly-(quaternary phosphonium) Oligochitosan.

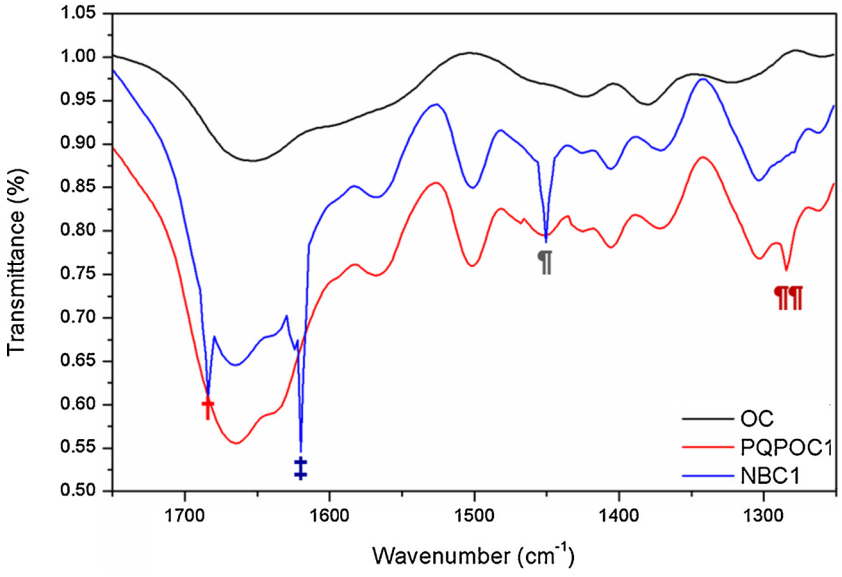

Fig. 1. Selected FTIR spectral regions for oligochitosan (OC), poly quaternary phosphonium chloride oligochitosan ($PQPOC_1$) and nano-biocomposite1 (NBC1, $PQPOC_1$ capped AgNPs). Stretching vibrations ascribed to: †, carbonyl group formed due to oxidation of phenolic or glycosidic hydroxyl; ‡, red-shift and demasking of imine; ¶, AgNPs and ¶¶, aryl-O (For interpretation of the references to colour in this figure legend, the reader is referred to the web version of this article.).

the spectra of NBC1 in comparison to that of parent $PQPOC_1$ confirming the pivotal role of phenolic and alcoholic OH groups in reduction of Ag^+ ions and stabilization of AgNPs. Meanwhile, a remarkable diminishing in the intensity of Aryl–O stretch in the spectra of NBCs along with the growth of new peak at ~1683 cm^{-1} which can recognized as carbonyl stretching mode confirming the oxidation of

phenolic or glycosidic hydroxyl group. This conclusion is in good agreement with the earlier outputs of Wang et al. work (Wang, Shao et al., 2014, 2014b). Moreover, a red-shift of the azomethine stretching vibration ($\Delta\nu$ = *ca.* -10 cm^{-1}) is derived from the involvement of azomethinic N-atom in the coordination of Ag^{+} ions and stabilization of AgNPs. Interestingly, observation of a new sharp band in the spectra of NBCs at 1450 ± 1 cm^{-1}, characteristic for AgNPs, evidence the formation and capping of Ag-NPs by PQPOCs.

3.4. NMR spectroscopy

^{1}H-NMR spectra of PQPOCs were recorded in 1% CD_3COOD/D_2O at 70 °C and are in good agreement with a successful surface-functionalization of OC with PQP brushes as revealed from the observation of highly de-shielded (downfield) singlets at the ranges of δ = 10.29-10.26 and 8.11-8.10 ppm characteristic for the resonance of phenolic and amide protons, respectively, engaged in an intramolecularly H-bonded environment. Meanwhile, ^{13}C-NMR spectra of PQPOCs offer further evidence for successful synthesis protocol as detected from notice of two sets of ^{13}C-NMR peaks; (i) A downfield set at (175, ~165, ~163 and range of 161-105 ppm) characteristic for the carbonyl, iminic, phenolic carbons and carbon skeleton of 3-(4-acetyl-3-hydroxyphenoxy)propyl)triphenylphosphonium segments, respectively. (ii) An up-field ^{13}C-NMR set in the range of 87-18 ppm ascribed to the resonances of carbon backbone of OC confirming the retention of its structural identity even after its surface modification. Finally the presence of hexafluorophosphate anion on the surface of $PQPOC_2$ was authenticated by the observation of a septet centered at -144.19 ppm and a doublet centered at -70.13 ppm in the ^{31}P/ ^{19}F NMR spectra of $PQPOC_2$.

3.5. UV–vis absorption spectra

The UV–vis absorption spectra (Fig. 2) demonstrate a divergence between the as-synthesized AgNPs obtained using different PQPOCs. Where the symmetrical surface plasmon resonance (SPR) peak observed around 400 nm was significantly grown for AgNPs prepared and capped by $PQPOC_1$ in NBC_1 when compared with AgNPs obtained and enveloped by $PQPOC_2$ in NBC_2. Moreover, the growth of a new narrow and asymmetrical SPR absorbance peak around 530 nm, in the spectra of NBCs, provids a strong evidence for the successful formation and capping of AgNPs by PQPOCs. The difference in the UV–vis absorption spectra for different NBCs depending on the reducing and capping agents (PQPOCs) revealed that the structure of PQPOCs played important roles in size and shape-controlled synthesis of AgNPs.

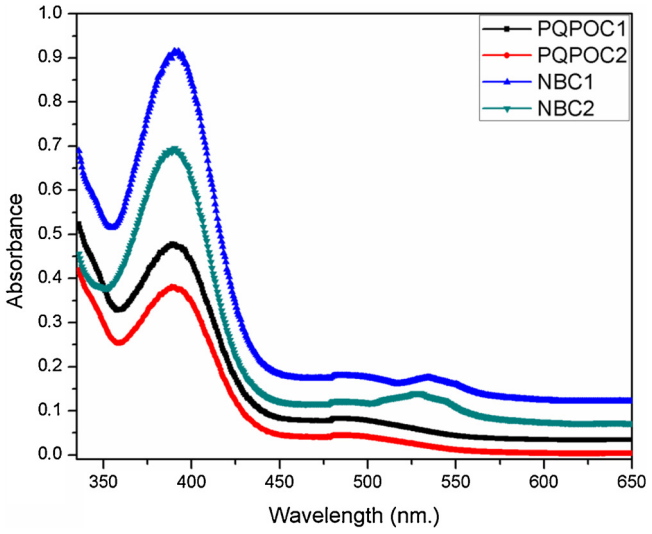

Fig. 2. UV–vis spectra of the PQPOCs and NBCs. The powdered samples (0.005 mg) are dissolved in 5 mL of deionized water and then each solution is monitored using UV–vis spectroscopy.

3.6. Morphological characterization

The surface microstructure of the as-synthesized NBCs ($PQPOC_1$-AgNPs and $PQPOC_2$-AgNPs) was investigated using SEM technique (Fig. 3A and D). It is clearly seen that the green-synthesized AgNPs with certain spherical shape are well dispersed on the surface of surface of $PQPOC_1$ and $PQPOC_2$ confirming their successful preparation. An additional evidence for formation and capping of AgNPs by PQPOCs was provided from energy dispersive x-ray (EDX) analysis, which reveals the existence of atomic Ag, C, O, N and Cl upon the surface of NBC_1 (Fig. 3C). On the other hand, there is many elements are observed upon the surface of NBC_2 including atomic Ag, C, N, F, P and O (Fig. 3F). These data are clarifying the successful preparation of NBC_1 and NBC_2 in pure form.

As shown in the transmission electron microscopy (TEM) images of NBCs (Fig. 3B and E), AgNPs were spherical in shape and dispersed within quite a narrow size distribution, which coincides with the UV–vis result. The surface of the AgNPs was tightly covered by PQPOCs, which prevented the aggregation of nanoparticles.

3.7. Cytotoxicity

The cytotoxic effects two nano-biocomposites (NBC1 and NBC2) towards Vero cells was investigated using MTT assay. It noticed that NBC1 is less cytotoxic than NBC2 as revealed from the maximum nontoxic concentration (MNTC) values ($MNTC_{NBC1}$ = 200 µL/mL, $MNTC_{NBC2}$ = 220 µL/mL). Thus when Vero cells treated with serial concentrations of NBC1 (up to 200 µL/mL) and NBC2 (up to 220 µL/mL), no morphological changes were observed in these cells and consequently no inhibition of their enzyme activity.

3.8. Antiviral activity

3.8.1. Single dose antiviral performance

The antiviral activity of PQPOCs ($PQPOC_1$ & $PQPOC_2$) and NBCs (NBC1,2) have been evaluated at the concentration of (100 µL/mL). It was found that the lowest percentages of viral reduction 10.57%, 7.25% and 16% were observed with $PQPOC_2$ against virions of FCV, HAV, and CoxB4, respectively with log reduction 0.74 ± 0.30, 0.58 ± 0.21 and 1.12 ± 0.17 $TCID_{50}$/mL of initial viral titers of the three viruses, respectively (Fig. 4). While the antiviral activity of $PQPOC_1$ showed the significant log reduction of 1.48 ± 0.08, 1.35 ± 0.043, and 2.90 ± 0.100 $\log_{10}$ $TCID_{50}$/ml (by the 21.1%, 16.91%, and 41.42% reduction percentages against FCV, HAV, and CoxB4, respectively.

On the other hand, NBC2 showed higher antiviral activity than PQPOCs with 4.43 ± 0.04, 2.56 ± 0.05, and 4.84 ± 0.18 $\log_{10}$ $TCID_{50}$/mL and the reduction percentages of FCV, HAV, and CoxB4 were 63.38%, 31.96%, and 69.19%, respectively. Notworthy, the treatment with the NBC1 shows the strongest virucidal activity as the reduction titers were 5.64 ± 0.22, 4.69 ± 0.15, and 5.88 ± 0.08 $\log_{10}$ $TCID_{50}$/mL and reduction% of FCV, HAV, and CoxB4 were 80.62%, 58.65%, and 84.04%, respectively.

From our study, the novel prepared NBCs (NBC1,2) exhibited stronger antiviral activity, in comparison to PQPOCs ($PQPOC_1$ & $PQPOC_2$), against all the tested viruses. The enhanced antiviral efficacies of NBC's as a result of embedding AgNPs into the matrix of PQPOCs could be attributed to the ability of AgNPs to strongly interact with the viral glycoproteins, thereby preventing the viral invasion to the host cell (Mori et al., 2013). To get more insights regarding the potential role and mode of antiviral action for AgNPs embedded in NBCs, the effects of the concentration, morphological and physical features of AgNPs on the antiviral activity of NBCs will be investigated

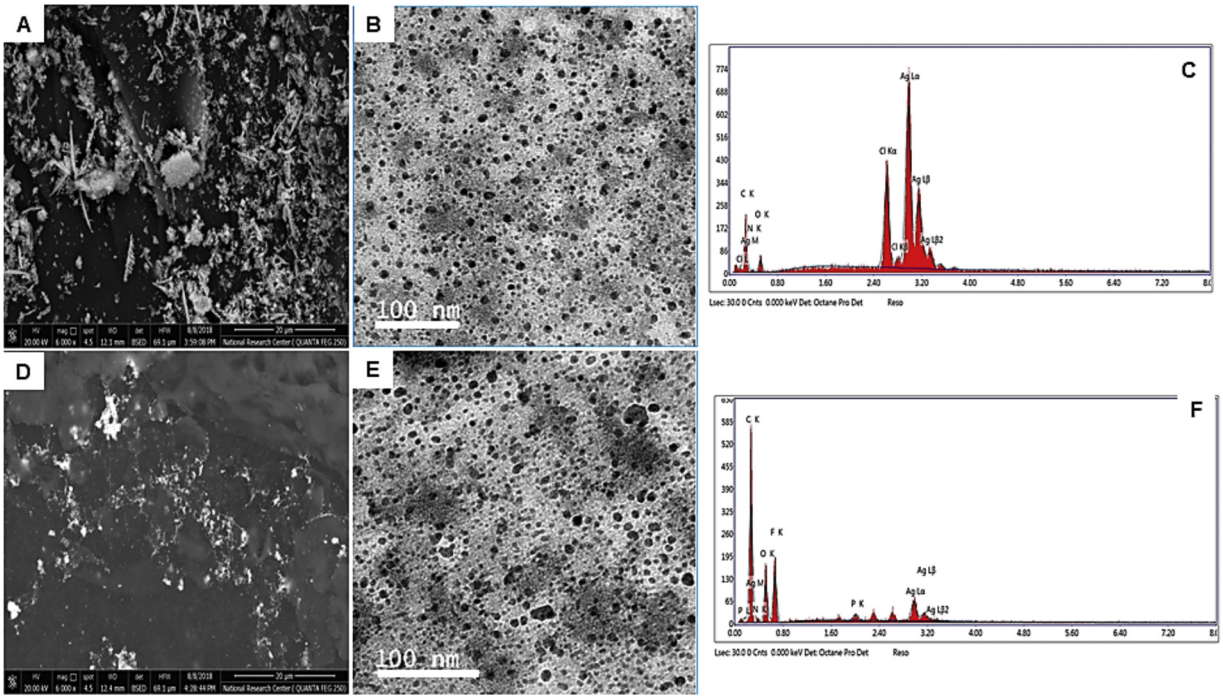

Fig. 3. (B and E) TEM images, (A and D) SEM images, and (C and F) EDX of NBC1 and NBC2, respectively.

in the future work. Our trend of results was in good consistency with the previous studies which revealed that the incorporation nanomaterials into a pharmacological formulation had significantly enhanced its biocidal activity (Kim et al., 2007; Morones et al., 2005).

3.8.2. Effect of NBC concentrations of its antiviral performance

The NBC1 showed a virucidal effect against all tested viruses with concentration-dependent activities profile. Where its activity in the reduction of infectious FCV virions at different level of concentrations (50, 100, and 150 µL/mL) are 3.83 ± 0.056, 5.64 ± 0.22, and 6.44 ± 0.17 $\log_{10}$ $TCID_{50}$/mL corresponding to 54.66%, 80.62%, and 92.05% of the reduction%, respectively (Fig. 5). Also, the antiviral effect of the NBC1 against HAV showed a highly significant reduction by 2.37 ± 0.045, 4.69 ± 0.15, and 7.05 ± 0.21 $\log_{10}$ $TCID_{50}$/mL corresponding to 29.62%, 58.62%, and 88.12% reduction%, respectively (Fig. 5). On the other hand, the maximum antiviral activity of NBC1was detected against CoxB4 with reduction of 4.33 ± 0.09, 5.88 ± 0.08, 7 ± 0.00 $TCID_{50}$/mL corresponding to 61.85%, 84.04%, and 100%, respectively (Fig. 5).

3.8.3. Effect of pH upon the virucidal activity of NBC1

Effect of pH on the antiviral activity of NBC1 is depicted in Fig. 6 which showed a highly statistically significant difference of antiviral efficacies against FCV, HAV, and CoxB4 at different pH values ($P \leq 0.001$). The obtained results clearly showed that at pH 4, the antiviral activity of NBC1 has reached the maximum level as revealed from the sharp diminishing in the titer of the inoculated viruses compared to other pH values. Contrary, this lower pH exert a very mild effect on the control samples of where the viruses titers were reduced by, 0.46 ± 0.22, 0.21 ± 0.31 and 0.35 ± 0.28 log10 $TCID_{50}$/mL for FCV, HAV, and CoxB4, respectively at pH 4. Also, at pH 6 the antiviral effect of composite was strong against all tested viruses, with the titers recovery of 0.56 ± 0.04, 0.86 ± 0.03, and 0.46 ± 0.03 $\log_{10}$ $TCID_{50}$/mL corresponding to 8%, 10.78%, and 6.56% respectively, from the initially inoculated titers of FCV, HAV and CoxB4 (10^7, 10^8 and 10^7 $TCID_{50}$/mL, respectively), with no effect on control virions. At neutral pH, NBC1 exhibited good antiviral activity as noticed from the recoded titers values of FCV, HAV and CoxB4 (1.53 ± 0.02, 2.59 ± 0.02, 0.95 ± 0.04 $\log_{10}$ $TCID_{50}$/mL corresponding to 21.8%, 32.14%, and 13.56%, respectively), while, no significant reduction was observed for

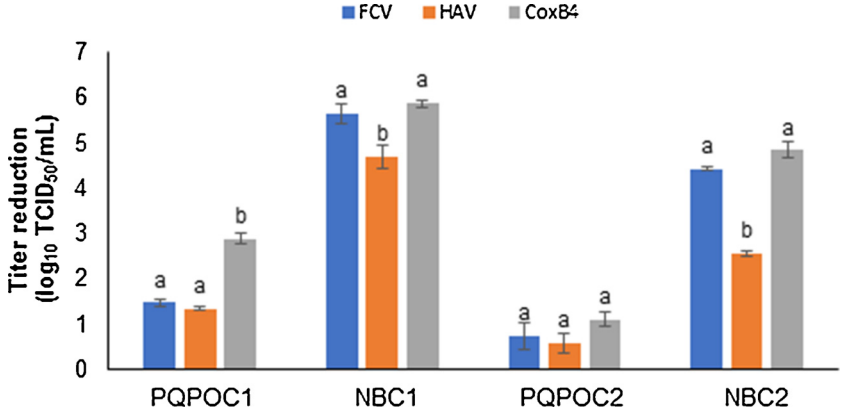

Fig. 4. Titer reduction of FCV, HAV, and CoxB4 treated with PQPOCs ($PQPOC_1$ & $PQPOC_2$) and NBCs (NBC1,2) at the concentration (100 µL/mL), as detected by $\log_{10}$ $TCID_{50}$/mL.

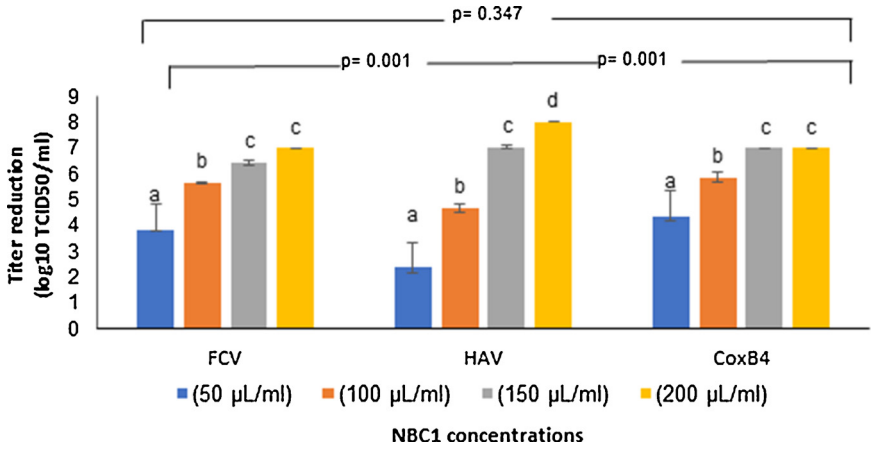

Fig. 5. Infectious titer reduction of FCV, HAV, and CoxB4 after treatment with different concentrations (50, 100, 150, and 200 µL/mL) of NBC1, as detected by $\log_{10}$ $TCID_{50}$/mL (where letters (a, b, c, d) to show which bars are significantly different).

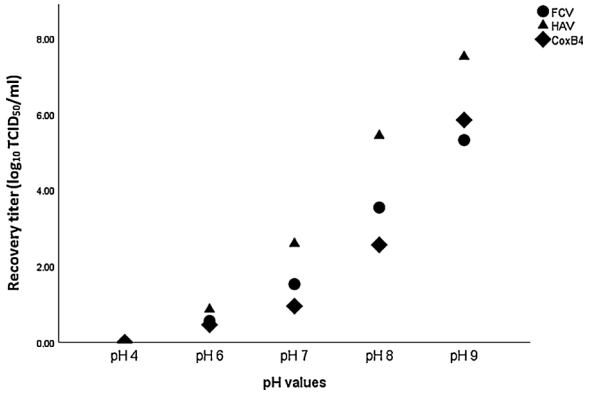

Fig. 6. FCV, HAV and CoxB4 titers treated with NBC1 at different pH values (4, 6, 7, 8, and 9) as detected by $\log_{10}$ $TCID_{50}$/mL.

virions in the NBC1-free tubes (controls) at neutral pH. Contrary, NBC1 has moderate virucidal activity at slight basic pH 8 as shown from the titers of FCV, HAV and CoxB4 at this pH which was found to be 3.54 ± 0.06, 5.43 ± 0.07 and 2.56 ± 0.12 $\log_{10}$ $TCID_{50}$/mL with recovery% of 50.57%, 67.91%, and 36.57%, respectively, however, the viral reduction in the controls tubes was found to be 0.96 ± 0.23, 0.22 ± 0.04 and 0.54 ± 0.2 $TCID_{50}$/mL for FCV, HAV, and $CoxB_4$, respectively at this pH, negligible effect. Meanwhile, stronger basic medium (pH 9) the antiviral activity of NBC1 was feeble (titers values of FCV, HAV and CoxB4 for treated samples are 5.31 ± 0.08, 7.51 ± 0.13, and 5.84 ± 0.20 $\log_{10}$ $TCID_{50}$/mL with recovery% 75.9, 93.87%, and 83.47%, respectively), while for controls are 1.78 ± 0.32, 0.38 ± 0.01 and 0.97 ± 0.11 $\log_{10}$ $TCID_{50}$/mL, respectively. Thus, our findings indicated that the antiviral activity of NBC1 was pH-dependent.

The fluctuation of the antiviral efficacies for NBCs by changing pH can be ascribed several possible mechanisms; (i) The acidic pH enhances the aqueous solubility of the AgNPs enveloping agents, PQPOCs, allowing more free and accessible AgNPs for virus interaction. These capping agents may prevent or weaken the interaction between virions and AgNPs due to their spatial restriction (Mori et al., 2013). (ii) The lower pH may induce conformational changes in the viral membrane fusion proteins and thereby activates their intrinsic fusion activity. (iii) Lower pH may also play a crucial in triggering capsid uncoating (Greber, Singh, & Helenius, 1994).

3.8.4. Proposed mechanism for antiviral action of NBC1

Thus, the use of AgNPs has been extended to the development of antiviral treatments that inhibit or even reduce their infection, including their attachment and penetration (Galdiero et al., 2011). Moreover, Kochkina, Chirkov and others have proposed that CS may trigger structural damage to the virus capsids causing inactivation as well as, blocking viral replication, where it can interact with the viral capsid negative charge (Kochkina & Chirkov, 2000; Su, Zivanovic, & D'Souza, 2009). Based upon these facts and other reported studies (Elechiguerra et al., 2005; Lara, Garza-Treviño, Ixtepan-Turrent, & Singh, 2011), we can suggest a preliminary mechanism for the antiviral action of our new NBCs as the AgNPs may prevent the association between the virus and the host cell based on the direct association of AgNPs with viral envelope glycoprotein, thereby inhibiting entry of the virus into host cells. Meanwhile, the inhibition of the viral propagation by PQPOC component of the NBC could be due to the interference with the capacity of tested viruses to infiltrate the target cells. Which may be attributed to either the direct damage the viral moieties or blocking viral entry. As the tested viruses (FCV, HAV, and CoxB4) belonged to the non-enveloped viruses, so they have no lipid coats to be attacked by polycation brushers on the surface of PQPOCs. Thus, it was assumed that PQPOC served as a viral interior inhibitor by blocking the interaction of targeted viruses with the host. We propose that the negatively-charged binding sites of tested viruses (portal-like form of C-terminal segment in FCV (Conley et al., 2019); oxyanion hole in CoxB4 (Baxter et al., 2006); few negative terminals in HAV (Wang et al., 2017)) were electrostatically interacted with for positive brushes of TPP fragments in PQPOC which significantly inactivates FCV and CoxB4 more than HAV, by blocking their cell entry. The significant enhancement in the antiviral activity by increasing the concentration of NBC, as revealed from the experimental results (*cf.* Fig. 5), provides strong evidence for the reasonableness of our suggestions. Moreover, the remarkable enhancement of the antiviral action of NBC1 at acidic medium (pH 4, see Section 3.8.3) provide strong evidence for this suggestion. Also, the CS skeleton in PQPOC can curb the propagation of viruses by different possible mechanisms (Chirkov, 2002): (a) Promoting ribonuclease activity which increases the degradation of viral RNA and consequently prevents its transcription and translation. (b) The glucosamine residue of CS may hinder the binding between the major viral coat protein (glycoprotein gp120) and their proper receptors.

4. Conclusion

This study reports the synthesis of poly quaternary phosphonium-based oligochitosans ($PQPOC_{1,2}$). PQPOCs were used as synergistic reductants for Ag(I) in preparation of silver nanoparticles (AgNPs) and capping agent to stabilize them through fabrication of PQPOCs-AgNPs nano-biocomposites (NBC1,2). The new materials were structurally and morphologically characterized based upon their spectral data (UV–vis,

FTIR, NMR), electron microscopic examination (SEM, TEM) and EDX analysis, as well. The outcomes of these spectroscopic and microscopic analyses revealed the successful formation PQPOCs, AgNPs and NBCs. Furthermore, the single-dose (100 μL/mL) antiviral performance of the PQPOCs and NBCs against common human enteric viruses (FCV, HAV, and CoxB4) reflects a higher virucidal activity for NBCs as compared with PQPOCs as revealed from the viral reduction% (Viral reduction = 21.1/41.42, 16.91/80.62, and 58.65/84.04%, for $PQPOC_1$/NBC1 against FCV, HAV, and CoxB4, respectively). To get an insight into the mechanism of the antiviral action of these new materials, the effect of concentration and pH on the antiviral effect of the most potent composite (NBC1) were assessed. It was found that the antiviral activity of NBC1 is concentration- and pH-dependent where NBC1 acquired its maximum antiviral at [NBC1] = 200 μL/mL and pH 4. The enhanced antiviral performance of NBCs could be attributed to multiple additive effects such as: (i) AgNPs could interact with the virions active sites (such as glycoproteins) and prevent viral attachment and penetration. (ii) PQPOC served as a viral interior inhibitor by blocking the interaction of targeted viruses with the host due to the electrostatic interactions between the positive brushes of PQPOC and negatively-charged binding sites of viruses. (iii) CS skeleton in PQPOC could induce ribonuclease to degrade the viral RNA and consequently prevents its transcription and translation. In conclusion, the current work initiates a promising strategy for preparation TPP-based CS/AgNPs composites which may lead to future integrated antiviral researches.

Appendix A. Supplementary data

Supplementary material related to this article can be found, in the online version, at doi:https://doi.org/10.1016/j.carbpol.2019.115261.

References

Antony, R., Arun, T., Theodore, S., & Manickam, D. (2019). A review on applications of chitosan-based Schiff bases. *International Journal of Biological Macromolecules, 129*(15), 615–633. https://doi.org/10.1016/j.ijbiomac.2019.02.047.

Baxter, N. J., Roetzer, A., Liebig, H.-D., Sedelnikova, S. E., Hounslow, A. M., Skern, T., et al. (2006). Structure and dynamics of coxsackievirus B4 2A proteinase, an enyzme involved in the etiology of heart disease. *Journal of Virology, 80*, 1451–1462. https://doi.org/10.1128/JVI.80.3.1451-1462.2006.

Biswas, S., Dodwadkar, N. S., Piroyan, A., & Torchilin, V. P. (2012). Surface conjugation of triphenyl-phosphonium to target poly(amidoamine) dendrimers to mitochondria. *Biomaterials, 33*, 4773–4782. https://doi.org/10.1016/j.biomaterials.2012.03.032.

Boddapati, S. V., Tongcharoensirikul, P., Hanson, R. N., D'Souza, G. G. M., Torchilin, V. P., & Weissig, V. (2005). Mitochondriotropic liposomes. *Journal of Liposome Research, 15*, 49–58. https://doi.org/10.1081/LPR-64958.

Bui, V. K. H., Park, D., & Lee, Y.-C. (2017). Chitosan combined with ZnO, TiO_2 and Ag nanoparticles for antimicrobial wound healing applications: A mini review of the research trends. *Polymers. 9*, 1–24. https://doi.org/10.3390/polym9010021.

Chirkov, S. N. (2002). The antiviral activity of chitosan (Review). *Applied Biochemistry and Microbiology, 38*, 1–8. https://doi.org/10.1023/A:1013206517442.

Conley, M. J., Mcelwee, M., Azmi, L., Gabrielsen, M., Byron, O., Goodfellow, I. G., et al. (2019). Calicivirus VP2 forms a portal-like assembly following receptor engagement. *Nature Letter, 565*, 377–383. https://doi.org/10.1038/s41586-018-0852-1.

Chen, N., Zheng, Y., Yin, J., Li, X., & Zheng, C. (2013). Inhibitory effects of silver nanoparticles against adenovirus type 3 in vitro. *Journal of Virological Methods, 193*, 470–477. https://doi.org/10.1016/j.jviromet.2013.07.020.

D'Souza, D. H., Sair, A., Williams, K., Papafragkou, E., Jean, J., Moore, C., et al. (2006). Persistence of caliciviruses on environmental surfaces and their transfer to food. *International Journal of Food Microbiology, 108*, 84–91. https://doi.org/10.1016/j.ijfoodmicro.2005.10.024.

Durán, N., Nakazato, G., & Seabra, A. B. (2016). Antimicrobial activity of biogenic silver nanoparticles, and silver chloride nanoparticles: An overview and comments. *Applied Microbiology and Biotechnology, 100*, 6555–6570. https://doi.org/10.1007/s00253-016-7657-7.

EFSA (2016). The European Union summary report on trends and sources of zoonoses, zoonotic agents and food-borne outbreaks in 2015. *EFSA J. 14*. https://doi.org/10.2903/j.efsa.2016.4634.

Elechiguerra, J., Burt, J. L., Morones, J. R., Camacho-Bragado, A., Gao, X., Lara, H. H., & Yacaman, M. (2005). Interaction of silver nanoparticles with HIV-1. *Journal of Nanobiotechnology, 3*, 6–15. https://doi.org/10.1186/1477-3155-3-6.

El-Mohamady, R. S., Ghattas, T. A., Zawrah, M. F., & Abd El-Hafeiz, Y. G. M. (2018). Inhibitory effect of silver nanoparticles on bovine herpesvirus-1. *International Journal of Veterinary Science and Medicine, 6*, 296–300. https://doi.org/10.1016/j.ijvsm.2018.09.002.

Elshaarawy, R. F. M., Refaee, A. A., & El-Sawi, E. A. (2016). Pharmacological performance of novel poly-(ionic liquid)-grafted chitosan-N-salicylidene Schiff bases and their complexes. *Carbohydrate Polymers, 146*, 376–387. https://doi.org/10.1016/j.carbpol.2016.03.017.

Elshaarawy, R. F. M., Mustafa, F. H. A., Herbst, A., Farag, A. E. M., & Janiak, C. (2016). Surface functionalization of chitosan isolated from shrimp shells, using salicylaldehyde ionic liquids in exploration for novel economic and ecofriendly antibiofoulants. *RSC Advances, 6*, 20901–20915. https://doi.org/10.1039/c5ra27489c.

Elshaarawy, R. F. M., Dechnik, J., Hassan, H. M. A., Dietrich, D., Betiha, M. A., Schmidt, S., et al. (2018). Novel high throughput mixed matrix membranes embracing poly ionic liquid-grafted biopolymer: Fabrication, characterization, permeation and antifouling performance. *Journal of Molecular Liquids, 266*, 484–494. https://doi.org/10.1016/j.molliq.2018.06.100.

Elshaarawy, R. F. M., & Janiak, C. (2014). Toward new classes of potent antibiotics: Synthesis and antimicrobial activity of novel metallosaldach-imidazolium salts. *European Journal of Medicinal Chemistry, 75*, 31–42. https://doi.org/10.1016/j.ejmech.2013.09.029.

Elshaarawy, R. F. M., Mustafa, F. H. A., van Geelen, L., Abou-Talebe, A. E. A., Tadrose, H. R. Z., Kalscheuerd, R., et al. (2017). Mining marine shell wastes for polyelectrolyte chitosan anti-biofoulants: Fabrication of high-performance economic and ecofriendly anti-biofouling coatings. *Carbohydrate Polymers, 172*, 352–364. https://doi.org/10.1016/j.carbpol.2017.05.059.

Gaikwad, S., Ingle, A., Gade, A., Rai, M., Falanga, A., Incoronato, N., et al. (2013). Antiviral activity of mycosynthesized silver nanoparticles against herpes simplex virus and human parainfluenza virus type 3. *International Journal of Nanomedicine, 8*, 4303–4314. https://doi.org/10.2147/IJN.S50070.

Gaillet, S., & Rouanet, J. M. (2015). Silver nanoparticles: Their potential toxic effects after oral exposure and underlying mechanisms–A review. *Food and Chemical Toxicology, 77*, 58–63. https://doi.org/10.1016/j.fct.2014.12.019.

Galdiero, S., Falanga, A., Vitiello, M., Cantisani, M., Marra, V., & Galdiero, M. (2011). Silver nanoparticles as potential antiviral agents. *Molecules, 16*, 8894–8918. https://doi.org/10.1142/9789814520652_0015.

Greber, U. F., Singh, I., & Helenius, A. (1994). Mechanisms of virus uncoating. *Trends in Microbiology, 2*(2), 52–56. https://doi.org/10.1016/0966-842X(94)90126-0.

Guan, G., Kim, S. W., Lin, Y., Tian, Y., Liu, G., & Wang, H. (2019). Biological effects and applications of chitosan and chito-oligosaccharides. *Frontiers in Physiology*. https://doi.org/10.3389/fphys.2019.00516 In press.

Gulati, B. R., Allwood, P. B., Hedberg, C. W., & Goyal, S. M. (2001). Efficacy of commonly used disinfectants for the inactivation of calicivirus on strawberry, lettuce, and a food-contact surface. *Journal of Food Protection, 64*, 1430–1434. https://doi.org/10.4315/0362-028X-64.9.1430.

Haas, C. N., Rose, J. B., Gerba, C., & Regli, S. (1993). Risk Assessment of virus in drinking water. *Risk Analysis, 13*, 545–552. https://doi.org/10.1111/j.1539-6924.1993.tb00013.x.

Jimenez, L., & Chiang, M. (2006). Virucidal activity of a quaternary ammonium compound disinfectant against feline calicivirus: A surrogate for norovirus. *American Journal of Infection Control, 34*, 269–273. https://doi.org/10.1016/j.ajic.2005.11.009.

Kalaivani, R., Maruthupandy, M., Muneeswaran, T., Beevi, A. H., Anand, M., Ramakritinan, C. M., et al. (2018). Synthesis of chitosan mediated silver nanoparticles (Ag NPs) for potential antimicrobial applications. *Frontiers in Laboratory Medicine, 2*, 30–35. https://doi.org/10.1016/j.flm.2018.04.002.

Khandelwal, N., Kaur, G., Kumar, N., & Tiwari, A. (2014). Application of silver nanoparticles in viral inhibition: A new hope for antivirals. *Digest Journal of Nanomaterials and Biostructures, 9*, 175–186.

Kim, J. S., Kuk, E., Yu, K. N., Kim, J.-H., Park, S. J., Lee, H. J., et al. (2007). Antimicrobial effects of silver nanoparticles. *Nanomedicine: Nanotechnology, Biology and Medicine, 3*, 95–101. https://doi.org/10.1016/j.nano.2006.12.001.

Kochkina, Z. M., & Chirkov, S. N. (2000). Effect of chitosan derivatives on the reproduction of coliphages T2 and T7. *Microbiology, 69*, 208–211. https://doi.org/10.1007/BF02756200.

Lara, H. H., Garza-Treviño, E. N., Ixtepan-Turrent, L., & Singh, D. K. (2011). Silver nanoparticles are broad-spectrum bactericidal and virucidal compounds. *Journal of Nanobiotechnology, 9*, 30–37. https://doi.org/10.1186/1477-3155-9-30.

Leon-Silva, S., Fernandez-Luqueno, F., & Lopez-Valdez, F. (2016). Silver nanoparticles (AgNPs) in the environment: A review of potential risks on human and environmental health. *Water, Air, and Soil Pollution, 227*. https://doi.org/10.1007/s11270-016-3022-9 306-225.

Lodder, W. J., van den Berg, H. H., Rutjes, S. A., & de Roda Husman, A. M. (2010). Presence of enteric viruses in source waters for drinking water production in the Netherlands. *Applied and Environmental Microbiology, 76*, 5965–5971. https://doi.org/10.1128/AEM.00245-10.

Lu, L., Sun, R. W., Chen, R., Hui, C. K., Ho, C. M., Luk, J. M., et al. (2008). Silver nanoparticles inhibit hepatitis B virus replication. *Antiviral Therapy, 13*, 253–262.

Mori, Y., Ono, T., Miyahira, Y., Nguyen, V. Q., Matsui, T., & Ishihara, M. (2013). Antiviral activity of silver nanoparticle/chitosan composites against H1N1 influenza A virus. *Nanoscale Research Letters, 8*, 93. https://doi.org/10.1186/1556-276X-8-93.

Morones, J. R., Elechiguerra, J. L., Camacho, A., Holt, K., Kouri, J. B., Ramírez, J. T., et al. (2005). The bactericidal effect of silver nanoparticles. *Nanotechnology, 16*, 2346–2353. https://doi.org/10.1088/0957-4484/16/10/059/meta.

Mosmann, T. (1983). Rapid colorimetric assay for cellular growth and survival: Application to proliferation and cytotoxicity assays. *Journal of Immunological Methods, 65*, 55–63. https://doi.org/10.1016/0022-1759(83)90303-4.

Murugadoss, A., & Chattopadhyay, A. (2008). A green chitosan–silver nanoparticle composite as a heterogeneous as well as micro-heterogeneous catalyst. *Nanotechnology, 19*, 1–9. https://doi.org/10.1088/0957-4484/19/01/015603/meta.

Park, S., Ko, Y.-S., Lee, S. J., Lee, C., Woo, K., & Ko, G. (2018). Inactivation of influenza A virus via exposure to silver nanoparticle-decorated silica hybrid composites. *Environmental Science and Pollution Research, 25*, 27021–27030. https://doi.org/10.1007/s11356-018-2620-z.

Prevost, B., Lucas, F. S., Goncalves, A., Richard, F., Moulin, L., & Wurtzer, S. (2015). Large scale survey of enteric viruses in river and waste water underlines the health status of the local population. *Environment International, 79*, 42–50. https://doi.org/10.1016/j.envint.2015.03.004.

Randazzo, W., Fabra, M. J., Falcó, I., López-Rubio, A., & Sánchez, G. (2018). Polymers and biopolymers with antiviral activity: Potential applications for improving food safety. *Comprehensive Reviews in Food Science and Food Safety, 17*, 754–768. https://doi.org/10.1111/1541-4337.12349.

Ray, P. C., Yu, H., & Fu, P. P. (2009). Toxicity and environmental risks of nanomaterials: Challenges and future needs. *Journal of Environmental Science and Health, Part C, 27*, 1–35. https://doi.org/10.1080/10590500802708267.

Reed, L. J., & Muench, H. (1938). A simple method of estimating fifty percent endpoints. *American Journal of Epidemiology, 27*, 493–497. https://doi.org/10.1093/oxfordjournals.aje.a118408.

Rogers, J. V., Parkinson, C. V., Choi, Y. W., Speshock, J. L., & Hussain, S. M. (2008). A preliminary assessment of silver nanoparticle inhibition of monkeypox virus plaque formation. *Nanoscale Research Letters, 3*, 129–133. https://doi.org/10.1007/s11671-008-9128-2.

Shaheen, M. N. F., El-hadedy, D. E., & Ali, Z. I. (2019). Medical and microbial applications of controlled shape of silver nanoparticles prepared by ionizing radiation. *BioNanoScience,* 1–9. https://doi.org/10.1007/s12668-019-00622-2.

Sharma, V., Kaushik, S., Pandit, P., Dhull, D., Yadav, J. P., & Kaushik, S. (2019). Green synthesis of silver nanoparticles from medicinal plants and evaluation of their antiviral potential against chikungunya virus. *Applied Microbiology and Biotechnology, 103*, 881–891. https://doi.org/10.1007/s00253-018-9488-1.

Simões, C. M. O., Amoros, M., & Girre, L. (1999). Mechanism of antiviral activity of triterpenoid saponins. *Phytotherapy Research, 13*, 323–328. https://doi.org/10.1002/(SICI)1099-1573(199906)13:4<323::AID-PTR448>3.0.CO;2-C.

Snedecor, G. W., & Cochran, W. G. (1980). *Statistical methods* (7th ed.). Ames: Iowa State University Press.

Sofy, A. R., El-Dougdoug, K. A., Mousa, A. A., Salem, G. S. E. A., Hmed, A. A., & Ghalleb, A. R. (2018a). Hazards and prevalence of hepatitis A virus (HAV) and human norovirus (NoV) in leafy green vegetables from Egyptian farms. *The Journal of Microbiology, 8*, 74–89. https://doi.org/10.5923/j.microbiology.20180803.04.

Sofy, A. R., El-Dougdoug, K. A., Mousa, A. A., Salem, G. S. E. A., Hmed, A. A., & Ghalleb, A. R. (2018b). Prevalence of adenovirus and coxsackievirus B4 in fresh produce plants from Egypt. *International Journal of Virology and Molecular Biology, 7*, 11–25. https://doi.org/10.5923/j.ijvmb.20180701.02.

Su, X., Zivanovic, S., & D'Souza, D. H. (2009). Effect of chitosan on the infectivity of murine norovirus, feline calicivirus, and bacteriophage MS2. *Journal of Food Protection, 72*, 2623–2628. https://doi.org/10.4315/0362-028X-72.12.2623.

Trefry, J. C., & Wooley, D. P. (2013). Silver nanoparticles inhibit vaccinia virus infection by preventing viral entry through a macropinocytosis-dependent mechanism. *Journal of Biomedical Nanotechnology, 9*, 1624–1635. https://doi.org/10.1166/jbn.2013.1659.

Wang, X.-Y., Shao, N.-M., Zhang, Q., & Cheng, Y.-Y. (2014). Mitochondrial targeting dendrimer allows efficient and safe gene delivery. *Journal of Materials Chemistry B, 2*, 2546–2553. https://doi.org/10.1039/C3TB21348J.

Wang, X.-H., Peng, H.-S., Yang, L., You, F.-T., Teng, F., Tang, A.-W., et al. (2013). Poly-L-lysine assisted synthesis of core–shell nanoparticles and conjugation with triphenylphosphonium to target mitochondria. *Journal of Materials Chemistry B, 1*, 5143–5152. https://doi.org/10.1039/C3TB20884B.

Wang, X., Zhu, L., Dang, M., Hu, Z., Gao, Q., Yuan, S., et al. (2017). Potent neutralization of hepatitis A virus reveals a receptor mimic mechanism and the receptor recognition site. *PNAS, 114*, 770–775. https://doi.org/10.1073/pnas.1616502114.

Wang, Z., Xu, C., Zhao, M., & Zhao, C. (2014). One-pot synthesis of narrowly distributed silver nanoparticles using phenolic-hydroxyl modified chitosan and their antimicrobial activity. *RSC Advances, 4*, 47021–47030. https://doi.org/10.1039/c4ra06908k.

WHO (2015). *WHO estimates of the global burden of foodborne diseases: Foodborne disease burden epidemiology reference group 2007–2015.* Geneva: World Health Organization.

Yasumura, Y., & Kawakita, Y. (1963). Studies on SV40 in tissue culture-preliminary step for cancer research in vitro. *Nihon Risnsho, 21*, 1201–1215.

Yamada, Y., & Harashima, H. (2008). Mitochondrial drug delivery systems for macromolecule and their therapeutic application to mitochondrial diseases. *Advanced Drug Delivery Reviews, 60*, 1439–1462. https://doi.org/10.1016/j.addr.2008.04.016.

Zhang, Y., Shen, Y.-J., Teng, X.-Y., Yan, M.-Q., Bi, H., & Morais, P. C. (2015). Mitochondria-targeting nanoplatform with fluorescent carbon dots for long time imaging and magnetic field-enhanced cellular uptake. *ACS Applied Materials & Interfaces, 7*, 10201–10212. https://doi.org/10.1021/acsami.5b00405.

Zhou, J., Zhao, W.-Y., Ma, X., Ju, R.-J., Li, X.-Y., Li, N., et al. (2013). The anticancer efficacy of paclitaxel liposomes modified with mitochondrial targeting conjugate in resistant lung cancer. *Biomaterials, 34*, 3626–3638. https://doi.org/10.1016/j.biomaterials.2013.01.078.